SPECIAL TOPIC — Physics in micro-LED and quantum dots devices

A polarization mismatched p-GaN/p-$Al_{0.25}Ga_{0.75}N$/p-GaN structure to improve the hole injection for GaN based micro-LED with secondary etched mesa

Yidan Zhang(张一丹)[1,2], Chunshuang Chu(楚春双)[1,3,†], Sheng Hang(杭升)[1,2], Yonghui Zhang(张勇辉)[1,2], Quan Zheng(郑权)[4], Qing Li(李青)[4], Wengang Bi(毕文刚)[2], and Zihui Zhang(张紫辉)[1,2,‡]

[1] *State Key Laboratory of Reliability and Intelligence of Electrical Equipment, Hebei University of Technology, Tianjin* 300401, *China*
[2] *School of Electronics and Information Engineering, Hebei University of Technology, Key Laboratory of Electronic Materials and Devices of Tianjin, Tianjin* 300401, *China*
[3] *School of Electrical Engineering, Hebei University of Technology, Tianjin* 300401, *China.*
[4] *State Key Engineering Center of Flat-Panel-Display Glass and Equipment, Shijiazhuang* 050035, *China*

(Received 28 July 2022; revised manuscript received 20 September 2022; accepted manuscript online 19 October 2022)

A low hole injection efficiency for InGaN/GaN micro-light-emitting diodes (μLEDs) has become one of the main bottlenecks affecting the improvement of the external quantum efficiency (EQE) and the optical power. In this work, we propose and fabricate a polarization mismatched p-GaN/p-$Al_{0.25}Ga_{0.75}N$/p-GaN structure for 445 nm GaN-based μLEDs with the size of 40×40 μm^2, which serves as the hole injection layer. The polarization-induced electric field in the p-GaN/p-$Al_{0.25}Ga_{0.75}N$/p-GaN structure provides holes with more energy and can facilitate the non-equilibrium holes to transport into the active region for radiative recombination. Meanwhile, a secondary etched mesa for μLEDs is also designed, which can effectively keep the holes apart from the defected region of the mesa sidewalls, and the surface nonradiative recombination can be suppressed. Therefore, the proposed μLED with the secondary etched mesa and the p-GaN/p-$Al_{0.25}Ga_{0.75}N$/p-GaN structure has the enhanced EQE and the improved optical power density when compared with the μLED without such designs.

Keywords: μLED, polarization mismatch, secondary etched mesa, hole injection

PACS: 85.30.De, 85.35.Be, 85.60.Bt, 85.60.Jb **DOI:** 10.1088/1674-1056/ac9b35

1. Introduction

When compared with organic light-emitting diodes (LEDs), III-nitride based LEDs have advantages of low power consumption, long operation life-time, high luminous efficiency, quick response, etc.[1–3] Meanwhile, improved light extraction efficiency (LEE), better current spreading and enhanced heat dissipation can be further achieved by reducing the LED chip size, modifying the inclined sidewall angle and so on.[4–6] Thus, the micro-light emitting diodes (μLEDs) are considered as promising candidates in applications of implantable optoelectronic equipment, display, optical communication, biomedical detection, etc.[7] However, as the size of the LED chip becomes smaller, the external quantum efficiency (EQE) and the optical power decrease significantly,[8,9] which is due to the sidewall damages on the mesa. These surface damages are caused by the plasma-assisted dry etching process. They form carrier leakage channels and produce nonradiative recombination.[10,11] In order to reduce the influence of the defected region on the optoelectronic properties for GaN-based μLEDs, the surface and sidewall defects for μLEDs can be repaired by optimizing the chip fabrication process. For example, the defects on mesa sidewalls can be reduced by optimizing the annealing time and using chemical treatment.[12,13] Moreover, an insulation passivation layer, e.g., SiO_2 deposited by plasma-enhanced chemical vapor deposition (PECVD) or atomic layer deposition (ALD) systems, can also annihilate surface defects for μLEDs.[14,15] According to our recent report, a resistive ITO/p-GaN junction at the mesa edge for GaN-based μLEDs can function as a current blocking layer, and as a result, the holes can be kept apart from the mesa edge.[16] The current leakage and the surface recombination can be further decreased if one can both make a more resistive junction and generate the energy barriers simultaneously at the mesa periphery. For that goal, our group proposed an ITO/Ta_2O_5/p-GaN periphery junction at the μLED mesa edge.[17] The most significant advantage of this design is that the large relative dielectric constant of 26 for the Ta_2O_5 layer can generate energy barriers in the p-GaN layer, and this helps to confine the holes in the central region for the μLED mesa. According to the report by Kou *et al.*,[10] the hole injection can be promoted when the surface recombination can be significantly suppressed. Nevertheless, there is little possibility of completely eliminating the hole diffusion to the mesa edge. Hence, it becomes increasingly important that the hole injec-

†Corresponding author. E-mail: cs.chu@hebut.edu.cn
‡Corresponding author. E-mail: zh.zhang@hebut.edu.cn

© 2023 Chinese Physical Society and IOP Publishing Ltd

tion efficiency shall be enhanced for GaN-based μLEDs.

In this work, we design and fabricate a GaN-based μLED with a p-GaN/p-$Al_{0.25}Ga_{0.75}N$/p-GaN structure. Such p-GaN/p-$Al_{0.25}Ga_{0.75}N$/p-GaN structure can generate polarization-induced electric field that can help to make "hot" holes. In addition, a secondary etched mesa is also fabricated and passivated by using SiO_2 insulating layer. By doing so, the current can be effectively confined in the non-defected area, which suppresses the nonradiative recombination in the mesa edge. As a result, the hole injection can be improved while the surface nonradiative recombination can be decreased. This in turn improves the EQE and reduces the leakage current for the proposed μLED.

2. Structure design and parameters

In order to show the effectiveness of the proposed GaN-based μLED on the improvement for the optoelectronic characteristics, the epitaxial wafers for GaN-based μLEDs are grown on [0001]-oriented sapphire substrate by using metal-organic chemical vapor deposition (MOCVD) system. Both μLED wafers have a 2 μm thick GaN layer with the electron concentration of 5×10^{18} cm^{-3}. After that, 5 pairs of $In_{0.15}Ga_{0.85}N$/GaN multiple quantum wells (MQWs) are grown to produce the peak emission wavelength of ∼ 450 nm. The thicknesses of the quantum wells and the quantum barriers are ∼ 3 nm and ∼ 12 nm, respectively. Then, a 25 nm thick p-$Al_{0.25}Ga_{0.75}N$ electron blocking layer (p-EBL) with the hole concentration of 3×10^{17} cm^{-3} is utilized to reduce the electron leakage from MQWs. Next, an 80 nm thick p-GaN layer and a 10 nm thick p^+-GaN layer serve as the hole injection layer for the reference μLED wafer, for which the hole concentrations are estimated to be 3×10^{17} cm^{-3} and 1×10^{21} cm^{-3}, respectively. Nevertheless, different from the reference μLED wafer, the proposed μLED wafer has a 3 nm thick p-$Al_{0.25}Ga_{0.75}N$ layer with the hole concentration of 3×10^{17} cm^{-3} inserted into the p-GaN layer, so that a 30 nm p-GaN/3 nm p-$Al_{0.25}Ga_{0.75}N$/50 nm p-GaN structure can be formed. Different μLEDs have been fabricated such that devices A and B are made of the reference and the proposed μLED wafers in Figs. 1(a) and 1(b), respectively. The scanning electron microscope (SEM) image for the fabricated μLED is shown in Fig. 1(c). Details regarding the chip fabrication processes will be presented subsequently. We have conducted the cross-sectional transmission electron microscope (TEM) measurement in the p-type region for devices A and B that are presented in Figs. 1(d) and 1(e), respectively. We can see that the p^+-GaN layer, the p-GaN layer and the p-EBL are grown as the pre-set thickness for device A. Moreover, the thin p-$Al_{0.25}Ga_{0.75}N$ layer with the thickness of ∼ 3 nm has also been inserted into the p-GaN layer during the epitaxial growth process.

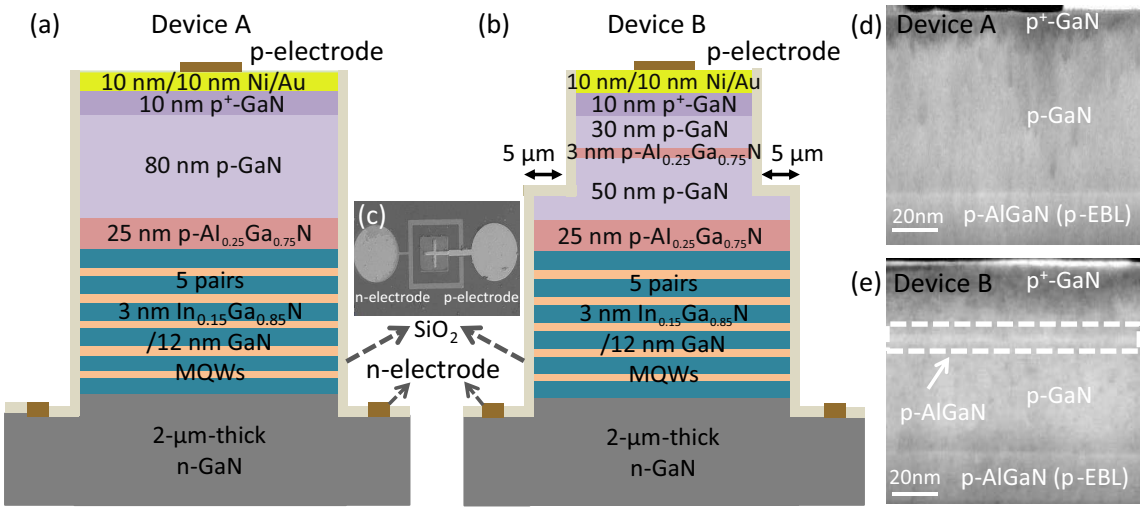


Fig. 1. Schematic diagrams for (a) device A and (b) device B with the p-GaN/p-$Al_{0.25}Ga_{0.75}N$/p-GaN structure and secondary etched mesa. (c) SEM image for the fabricated μLED with the chip size of 40×40 μm^2. Cross-sectional TEM images of the p-type region for (d) device A and (e) device B.

The fabrication processes for the two μLEDs are as follows. Firstly, for both devices, a square mesa is patterned and dry etched by using the inductively coupled plasma (ICP) system to expose the n-GaN layer. The mesa size is 40×40 μm^2 and the mesa height is 500 nm. Then, the secondary mesa for device B is etched on both sides of the p-type region. The height and the width for the secondary mesa are ∼ 60 nm and ∼ 30 μm, respectively. For both devices, the SiO_2 insulating layer of ∼ 200 nm is deposited on the mesa sidewalls by using PECVD system, which is used to passivate the sidewalls defects and isolate the contact between the p-electrode and the n-GaN layer. After patterning the SiO_2 insulating layer so that the metal contact regions can be exposed, a thin Ni/Au (10 nm/10 nm) is deposited on the p^+-GaN layer serving as the current spreading layer. The Ni/Au is annealed in the oxygen environment at the temperature of 450 °C for 3 min

to form the ohmic contact.[18] On the top of the Ni/Au current spreading layer, we deposit Ni/Au (10 nm/200 nm) so that the Ni/Au/Ni/Au p-type electrode is formed. Next, the Ti/Al/Ti/Au (20 nm/30 nm/60 nm/100 nm) is deposited on the n-GaN layer as the n-type ohmic contact.

The two μLEDs are numerically investigated by using APSYS software so that an in-depth understanding such as carrier transport and recombination processes can be obtained. The physical equations including Poisson's equation, Schrödinger equation, drift-diffusion equation, etc. are self-consistently solved.[19] The Shockley–Read–Hall (SRH) recombination lifetime is set to 100 ns and the Auger recombination coefficient is 1×10^{-30} cm^6/s in our model for the nonradiative recombination process.[20] The band offset ratio between the conduction band and valence band is set to 0.7/0.3 for the InGaN/GaN MQWs.[10] The LEE for the studied blue μLEDs is set to 60% by compromising our measured EQE and the reported value.[21] Additionally, we also set the defect model in our simulations. The electron trap level is set at 0.24 eV below the conduction band (i.e., $E_c - 0.24$ eV), for which the trap density and the capture cross section are 1×10^{13} cm^{-3} and 3.4×10^{-17} cm^2, respectively.[10,22] The hole trap level is set at 0.46 eV above the valence band (i.e., $E_v + 0.46$ eV), for which the trap density and the capture cross section are 1.6×10^{13} cm^{-3} and 2.1×10^{-15} cm^2, respectively.[10,23] Other important parameters in our simulation model can also be found in Ref. [24].

3. Results and discussion

By using a calibrated integrating sphere, we show the measured electroluminescence (EL) spectra in terms of various injection current densities for devices A and B in Figs. 2(a) and 2(b), respectively. Note, the measured devices are not packaged with bare μLED dies, so that only part of the photons can be collected by our optical fiber. It shows that the EL intensity for devices A and B increases as the current density increases from 50 A/cm^2 to 200 A/cm^2. Meanwhile, the EL intensity for device B is always stronger than that for device A at the same current density level. The inset in Fig. 2(a) shows the illuminating device taken under the optical microscope system. The blue emission with the peak wavelength of ~445 nm can be observed, which agrees with the set InN composition in the MQWs.

In order to better understand the impact of the proposed p-GaN/p-$Al_{0.25}Ga_{0.75}N$/p-GaN structure and the secondary etched mesa of the p-type region, we then experimentally and numerically obtain the EQE and optical power density at various injection current density levels for devices A and B in Figs. 3(a) and 3(b), respectively. We can see that the measured EQE and optical power density for device B are both

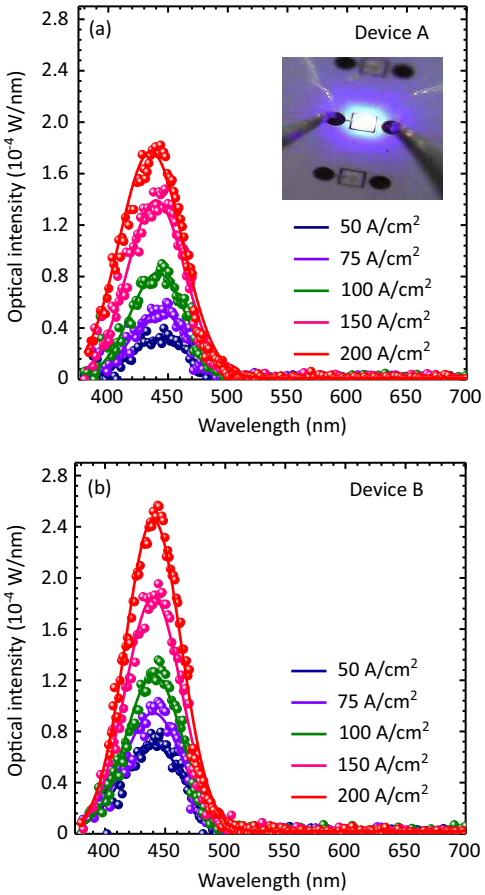


Fig. 2. Measured EL spectra for (a) device A and (b) device B at varying injection current density levels. The inset in (a) shows the image for the illuminating μLED at the current density of 200 A/cm^2.

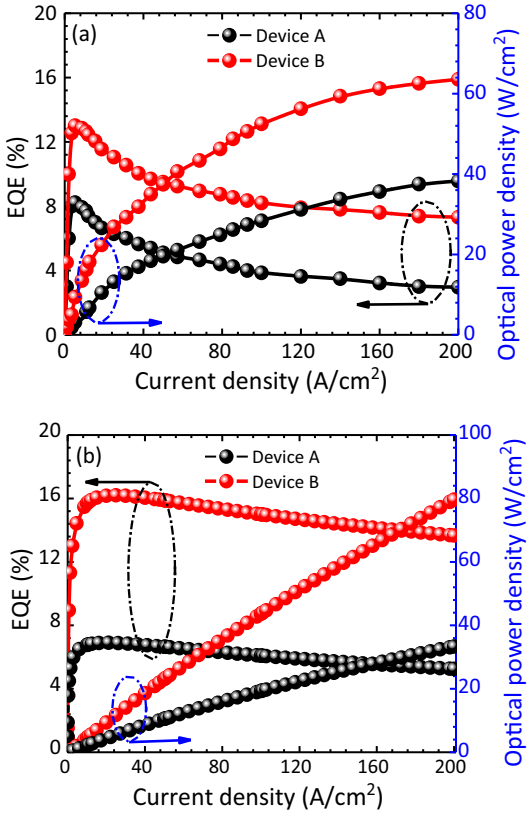


Fig. 3. (a) Measured and (b) calculated EQE and optical power density as a function of the injection current density for devices A and B, respectively.

higher than those for device A, which is consistent with the trend of the calculated results in Fig. 3(b). This also indicates the reliability of our simulation model. The results presented in Fig. 3(a) are also consistent with the EL profiles in Fig. 2. At the current density of 200 A/cm^2, the measured efficiency droop levels are 65.2% and 43.8% for devices A and B, respectively according to Fig. 3(a). These values are 23.7% and 15.6% for devices A and B, respectively according to the numerical results in Fig. 3(b). The reduced efficiency droop obtained both experimentally and numerically for device B can be well attributed to the increased hole injection.[25]

In order to reveal the underlying physical mechanism for the enhanced EQE and optical power for device B, we calculate the electric field and the hole concentration profiles for devices A and B in Figs. 4(a)–4(c), respectively. Figure 4(a) shows that the polarization electric field is formed at the multiple heterojunction interfaces for the p-GaN/p-$Al_{0.25}Ga_{0.75}N$/p-GaN structure. We define that the positive electric field is along the [0001] orientation. When we look into the electric field profile in the thin p-$Al_{0.25}Ga_{0.75}N$ layer, we can infer that the holes may lose energy as they travel through the thin p-$Al_{0.25}Ga_{0.75}N$ layer. To better investigate the net energy (W) that the holes obtain from the p-type region for devices A and B, we integrate the electric field by following the equation $W = e\int_0^l E_{\text{field}} \cdot \mathrm{d}x$, in which e is electron charge, E_{field} denotes the electric field profile and l represents the integration range. The values of W obtained by the holes are -0.09 eV and -0.18 eV for devices A and B at the current density of 200 A/cm^2, respectively. The negative value of W means that the holes obtain the energy from the p-type region and become "hot". Therefore, the injection of holes into the MQWs can be effectively promoted and the radiative recombination in the whole active region can be improved for device B according to Fig. 4(b). Figure 4(c) presents the lateral hole concentration distribution in the last quantum well closest to p-EBL. It shows that the hole concentration in the mesa sidewalls region of device B is lower than that of device A, while the hole concentration in the middle mesa region of device B is higher than that of device A.

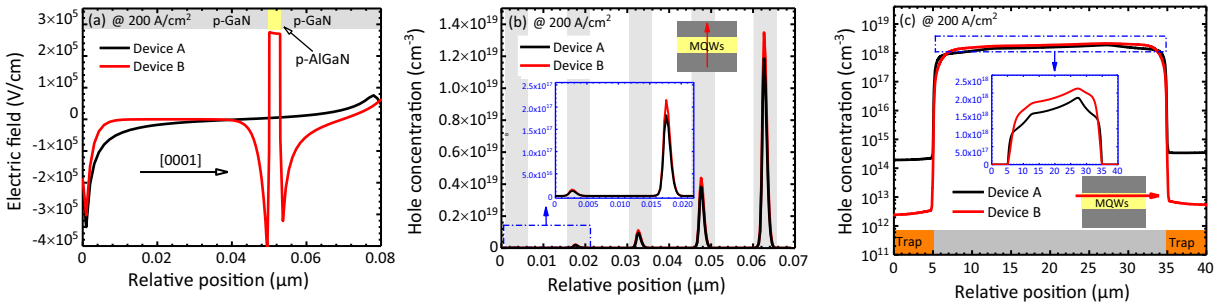


Fig. 4. (a) Numerically calculated electric field profiles for devices A and B with the p-GaN/p-$Al_{0.25}Ga_{0.75}N$/p-GaN. (b) Vertical hole concentration profiles in the MQW region and (c) lateral hole distribution in the last quantum well closest to the p-EBL for devices A and B. Data are calculated at the injection current density of 200 A/cm^2.

It is worth noting that the secondary etched mesa for device B also contains surface defects and these are also considered in our physical model. Hence, it is necessary to extract the recombination current for devices A and B. Figures 5(a) and 5(b) show the calculated radiative recombination current density and SRH recombination current density for devices A and B, respectively. According to Fig. 5(a), we can find that the radiative recombination for device B is significantly higher than that for device A. Nevertheless, Fig. 5(b) demonstrates that the SRH recombination current density for device A becomes larger. Note, the inset of Fig. 5(a) presents the lateral radiative recombination rate in the last quantum well closest to p-EBL for devices A and B. We can see that neither of the two devices has strong radiative recombination rate at the defected mesa edge, while the radiative recombination rate in the central mesa region is higher for device B thanks to the enhanced hole injection efficiency therein. The inset of Fig. 5(b) demonstrates that the defected mesa regions have a significant SRH nonradiative recombination rate. However, the secondary etched mesa helps suppress the SRH nonradiative recombination rate at the mesa edge for device B when compared with device A. Therefore, with the assistance of our physical calculations, we further confirm that the p-GaN/p-$Al_{0.25}Ga_{0.75}N$/p-GaN structure can produce hot holes and favor the hole injection into the MQW region. In the meanwhile, the secondary etched mesa can effectively suppress the SRH nonradiative recombination at the defected mesa edges. We also find that the newly generated surface defects at the secondary etched mesa edge sacrifice neither the hole injection nor the optical power.

It is known that the surface defects at the mesa sidewalls provide current leakage channels. Thus, the current–voltage (I–V) characteristics for the two μLEDs are measured and investigated, which are shown in Fig. 6. When the two μLEDs are reversed biased at the voltage of -5 V, the leakage current for device B is almost one order of magnitude smaller than that for device A. The on/off current ratios at the biases of -5 V and 5 V are 10^8 and 10^9 for devices A and B, respectively. The reduced leakage current and the increased on/off current ratio infer that device B can effectively suppress the surface

nonradiative recombination and reduce the leakage current on the mesa sidewalls. We also find that the forward voltage for device B is reduced when compared with device A, and this is due to the hot holes and the enhanced hole injection efficiency.

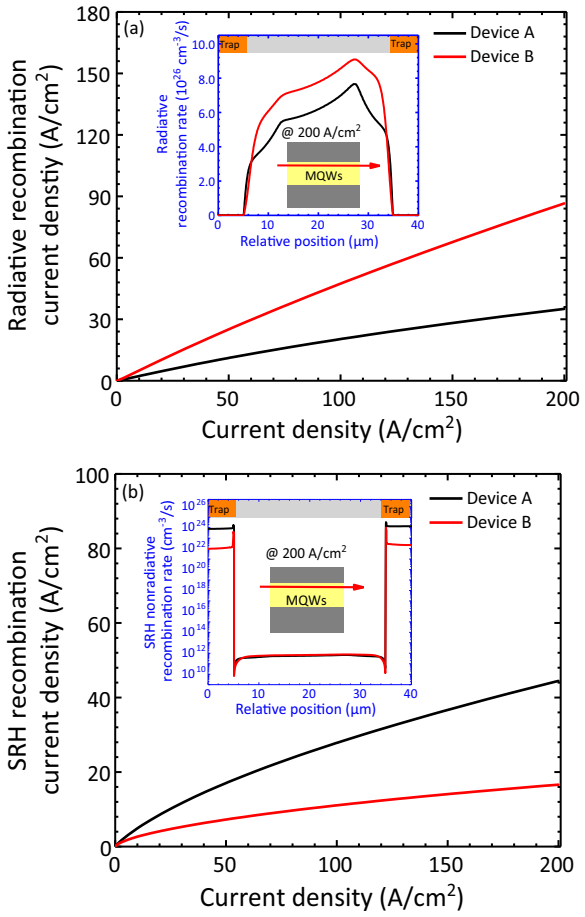


Fig. 5. (a) Radiative recombination current density and (b) SRH recombination current density as a function of injection current density for devices A and B. The insets in (a) and (b) show the lateral radiative recombination rate and the lateral SRH nonradiative recombination rate in the last quantum well closest to the p-EBL layer, respectively.

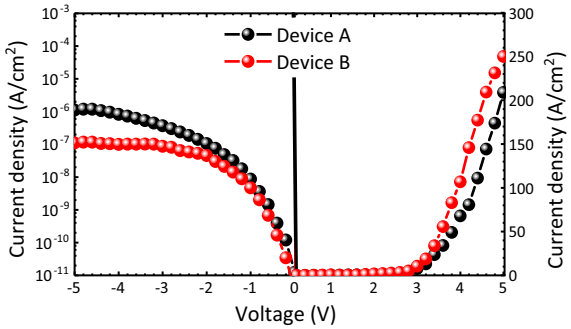


Fig. 6. Measured *I*–*V* characteristics in semi-log scale for devices A and B, respectively.

4. Conclusion

The secondary etched mesa and p-GaN/p-$Al_{0.25}Ga_{0.75}N$/p-GaN structure are proposed and the detailed analysis has been conducted for GaN-based μLEDs in this work. By using the p-GaN/p-$Al_{0.25}Ga_{0.75}N$/p-GaN structure, the polarization induced electric field therein can increase the kinetic energy for holes and hence the holes are more efficiently injected into the MQWs. For that reason, the EQE is increased by 155.6% at the current density of 200 A/cm^2 and the efficiency droop is suppressed to 43.8% for the proposed μLED. Meanwhile, the secondary etched mesa can also suppress the hole diffusion towards the mesa sidewalls and confine the holes into the central mesa region. Correspondingly, the surface SRH nonradiative recombination and the leakage current can be obtained and a high on/off current ratio of 10^9 can be generated for the proposed μLED. Therefore, we strongly believe that the findings in this work are very helpful for the community to better understand GaN-based μLEDs and the proposed structure paves a new way for making high-efficiency and strong-reliability GaN-based μLEDs.

Acknowledgments

This work was supported in part by the National Natural Science Foundation of China (Grant Nos. 62074050 and 61975051); Research Fund by State Key Laboratory of Reliability and Intelligence of Electrical Equipment, Hebei University of Technology (Grant Nos. EERI_PI2020008 and EERIPD2021012); and Joint Research Project for Tunghsu Group and Hebei University of Technology (Grant No. HI1909).

References

[1] Huang Y, Hsiang E L, Deng M Y and Wu S T 2020 *Light Sci. Appl.* **9** 105
[2] Zhang K, Liu Y, Kwok H and Liu Z 2020 *Nanomate* **10** 689
[3] Wu T, Sher C W, Lin Y, Lee C F, Liang S, Lu Y, Huang Chen S W, Guo W, Kuo H C and Chen Z 2018 *Appl. Sci.* **8** 1557
[4] Tian M, Yu H, Memon M H, Xing Z, Huang C, Jia H, Zhang H, Wang D, Fang S and Sun H 2021*Opt. Lett.* **46** 4809
[5] Yu H, Memon M H, Jia H, Zhang H, Tian M, Fang S, Wang D, Kang Y, Xiao S, Long S and Sun H 2022 *J. Semicond.* **43** 062801
[6] Hang S, Chuang C M, Zhang Y, Chu C, Tian K, Zheng Q, Wu T, Liu Z, Zhang Z H, Li Q and Kuo H C 2021 *Phys. D: Appl. Phys.* **54** 153002
[7] Zhou X, Tian P, Sher C W, Wu J, Liu H, Liu R and Kuo H C2020 *Progress in Quantum Electronics* **71** 100263
[8] Yu H, Memon M H, Wang D, Ren Z, Zhang H, Huang C, Tian M, Sun H and Long S 2021 *Opt. Lett.* **46** 3271
[9] Smith J M, Ley R, Wong M S, Baek Y H, Kang J H, Kim C H, Gordon M J, Nakamura S, Speck J S and DenBaars S P 2020 *Appl. Phys. Lett.* **116** 071102
[10] Kou J, Shen C C, Shao H, Che J, Hou X, Chu C, Tian K, Zhang Y, Zhang Z H and Kuo H C 2019 *Opt. Express* **27** A643
[11] Yu J, Tao T, Liu B, Xu F, Zheng Y, Wang X, Sang Y, Yan Y, Xie Z, Liang S, Chen D, Chen P, Xiu X, Zheng Y and Zhang R 2021 *Crystals* **11** 403
[12] Tian P, McKendry J J D, Gong Z, Guilhabert B, Watson I M, Gu E, Chen Z, Zhang G and Dawson M D 2012 *Appl. Phys. Lett.* **101** 231110
[13] Ley R T, Smith J M, Wong M S, Margalith T, Nakamura S, DenBaars S P and Gordon M J 2020 *Appl. Phys. Lett.* **116** 251104
[14] Wong M S, Hwang D, Alhassan A I, Lee C, Ley R, Nakamura S and DenBaars S P 2018 *Opt. Express* **26** 21324
[15] Chen W, Hu G, Lin J, Jiang J, Liu M, Yang Y, Hu G, Lin Y, Wu Z, Liu Y and Zhang B 2015 *Appl. Phys. Express* **8** 032102
[16] Hang S, Zhang M, Zhang Y, Chu C, Zhang Y, Zheng Q, Li Q and Zhang Z H 2021 *Opt. Express* **29** 31201

[17] Zhang M, Hang S, Chu C, Shao H, Zhang Y, Zhang Y, Zhang Y, Zheng Q, Li Q and Zhang Z H 2022 *IEEE Trans. Electron Devices* **69** 3213
[18] Koide Y, Maeda T, Kawakami T, Fujita S, Uemura T, Shibata N and Murakami M 1999 *J. Electron. Mater.* **28** 341
[19] Zhang Z H, Tiam Tan S, Kyaw Z, Ji Y, Liu W, Ju Z, Hasanov N, Wei Sun X and Volkan Demir H 2013 *Appl. Phys. Lett.* **102** 193508
[20] Meneghini M, Trivellin N, Meneghesso G, Zanoni E, Zehnder U and Hahn B 2009 *Appl. Phys.* **106** 114508
[21] Kirill A Bulashevich, Sergey S Konopllev and Sergey Y Karpov 2018 *Photonics* **5** 41
[22] Rigutti L, Castaldini A and Cavallini A 2008 *Phys. Rev.* **77** 045312
[23] Narita T, Tokuda Y and Kogiso T 2018 *Appl. Phys.* **123** 161405
[24] Vurgaftman I and Meyer J R 2003 *Appl. Phys.* **94** 3675
[25] Ni X, Fan Q, Shimada R, Özgür Ü and Morkoç H 2008 *Appl. Phys. Lett.* **93** 171113